Title: Land cover changes and its Implications on Urban Heat Island in Nairobi County: A GIS and Remote Sensing Approach.

Authors

Temitope Ezekiel Idowu[1, *, 2], Nelly Cherono Kiplangat[2], Rose Waswa[3]

1. Jomo Kenyatta University of Agriculture & Technology, Kenya, P O Box 62000-00200, Nairobi Kenya, 0718111621, lois.temitope@gmail.com.
2. Technical University of Kenya, P O Box 52428-00200, Nairobi Kenya, 0711652932, cherononelly34@gmail.com
3. Regional Centre for Mapping of Resources for Development, P O Box 632-00618, Nairobi Kenya, 0780447225, rwaswa@rcmrd.org

Abstract:

As cities expand and more megacities emerge, the impacts on the environment are increasingly becoming apparent. One of such impacts is the Urban Heat Island (UHI) phenomenon. Several studies have identified progressive vegetation losses and decrease in pervious surfaces as two of the main factors contributing to UHI. However, location-based studies help determine the pertinent contributing factors, thereby providing a valuable basis for the formulation of efficient mitigation strategies in such areas. This study investigated the impact of land cover changes on UHI and its evolution from the year 2000 to 2018 in Nairobi – a major city in East Africa. Medium resolution Landsat TM, ETM+ and OLI data were obtained for assessing the Land cover changes and establishing the relationship between the changes and the corresponding Land Surface Temperatures (LST). The datasets were acquired in intervals of 2002-2010-2018. A pixel-based supervised classification was used for assessing the land cover changes. The NDVI and emissivity for each LULC map were estimated. Final LST maps indicating the extents of UHI were developed from the emissivities and NDVI values using empirical equations. The results show that there was a direct link between the progression of LULC towards urbanisation and the increase in the LST in the study area from 2000 to 2018, i.e. as Nairobi became more urban it engendered higher of UHI values. The study also reveals that UHI is a dynamic phenomenon usually higher in dryer hotter months and lower in colder months.

Keywords: Urban Heat Island (UHI), Land surface temperature (LST), Vegetation Index, Land cover (LC) change, Urbanization, Remote sensing

*Corresponding author: Temitope Ezekiel Idowu

1.0 INTRODUCTION

The last two decades have seen a surge in the number of researches related to land cover changes, urbanisation and their ecological as well as social impacts. One of the identified global environmental changes is an observed rise in the near surface temperatures with an increase in urbanisation in different parts of the world. The phenomenon is widely referred to as the Urban Heat Island (UHI). The UHI phenomenon was studied and first described by Luke Howard in 1810 as a case where an area of land consistently experience temperatures higher than that of the surrounding area (Surawar & Kotharkar, 2017). Aleksandrowicz et al., (2017) termed UHI as the inclination towards experiencing temperature values up to 12 K higher than the surrounding rural periphery. The intensity of the UHI is invariably the temperature difference between the warmest zone in the urban area and the contiguous rural setting (Voogt & Oke, 2004). Global population trends show a bias towards urban migration. In a relatively short timeframe, the world's population residing in urban areas had passed 50% by 2018, and the percentage is expected to stand at 68% by 2050 (UN, 2018). Hence, the issue of UHI and its attendant effects cannot be taken lightly and according to Favretto, (2018) UHI should be regarded as a global challenge capable of negatively impacting the smooth running and habitability of the urban environments. The impacts of UHI may be felt in the areas of human health and comfort, urban planning, energy management, and urban air pollution.

UHI invariably increases peak energy demand and energy consumption in the form of increased electricity demand for cooling systems. This is evidenced by studies which reveal that for every 0.6 ℃ increase in ambient air temperatures, electricity requirement for cooling increases by 1.5 – 2 % at temperatures higher than 20 ℃, implying that 5 – 10% of the municipal demand for electricity goes into UHI compensation (Akbari, 2005). Other possible impacts of UHI include increased air pollutants and greenhouse gases emissions, thermal pollution in aquatic systems, discomfort and human health risks, alterations to local climate such as wind and rainfall patterns, fogs formation and humidity, and impaired water quality (EPA, 2019; Rinkesh, 2019).

The body of research on UHI has grown steadily in the past two decades with Asia leading the park in the number of studies done, while Africa is the least researched. Ngie et al., (2014) provides a comprehensive review of some few UHI related studies done in Africa and provides further insights on remote sensing approaches to the UHI study in the wake of the growth of megacities in the continent and the resulting energy and sustainability challenges. Two factors identified as significant causes or contributors to UHI are urbanisation and human activities due to the changes they induce on the physical characteristics of the earth's surface and the alterations to near-surface flow and radioactive fluxes. Physical parameters on the earth's surface which undergo the changes include the thermal capacity, albedo, moisture, and heat conductivity (Ngie et al., 2014). These changes occur because urbanisation and anthropogenic activities lead to the conversion of hitherto pervious and natural surfaces such as forests, and natural swarms into impervious surfaces like roads and cemented surfaces. Studies demonstrating how increases in impervious surfaces positively correlate with an increase in UHI are abundant in the literature (Madanian, et al., 2018;

Mohajerani, Bakaric, & Jeffrey-Bailey, 2017; Zhang, Ji, Shu, Deng, & Wu, 2008). Other causative factors with no less impact include the urban geometry (e.g. narrow streets and tall buildings); wind and cloud cover; climate and topography; and the changes in land use/land cover (LULC) patterns (Ngie et al., 2014).

When the geometry of the urban settings tends towards narrow streets and tall buildings, the ease of air circulation and wind flow are easily impeded. Unobstructed air movement and wind flow contribute to the cooling of the near-surface thereby reducing the build-up of UHI. Cloud cover and strong winds have been observed to reduce the impacts of UHI while clear skies and calmer winds achieve the opposite because they help make the most out of the solar energy hitting the surface and minimise surface heat being lost by convection (Kim & Baik, 2005). Climate and topography may also influence the formation of UHI. For instance, the presence of abundant water bodies close to an urban setting can produce cooling effects while mountain ranges may affect the local wind patterns in an area which will invariably impact UHI formation either positively or negatively. Finally, the spatial changes in LULC with respect to urbanization have been observed to have noticeable effects on UHI patterns in many studies with temperatures over built-up areas relatively higher than that of vegetative areas (Lo & Quattrochi, 2003; Obiefuna, Nwilo, Okolie, Emmanuel, & Daramola, 2018; Surawar & Kotharkar, 2017).

The oldest approach to the assessment of UHI has been with the use of fixed-thermometer networks for taking ground-based readings or the use of thermometers mounted on vehicles which form transverses and generates empirical data. This approach measures the air temperature at specific heights above the ground. A typical example is the 1973 study by Oke where data were gathered with the use of automobile transverses and then compared with previously published literature for establishing the relationship between city sizes and UHI (Oke, 1973) The second and relatively more recent and more widely used approach, is the use of satellite remote sensing. This approach involves the measurement of Land Surface Temperatures (LST) on the premise that all surfaces emit thermal energy in specific wavelength ranges. Sensors mounted on satellites can detect and take the readings of these wavelengths. It has therefore been established that satellite imagery is capable of providing measurements of energy reflecting and being emitted from different land surface types such as paved surfaces, roofs, water, bare ground and vegetation (Ngie et al., 2014). For instance, the Landsat Thematic Mapper (4, 5) and Enhanced Thematic Mapper plus (7) are multispectral images with bands 2, 3 and 4 used for land cover classification while the band 6 is a thermal band which can be used for determining the LST and subsequently identifying the UHI.

The advantages satellite remote sensing-based surface measurements hold over air measurements are its ability to provide more extensive spatial coverage, the comparatively low cost of imagery and the recent milestones made in image processing techniques. However, surface measurement approach is not without its limitations. The first limitation is that the images do not entirely capture the thermal emissions from vertical surfaces like the walls of tall buildings but only the horizontal surfaces like the rooftops (Goldreich, 2006). Another major challenge in the past is how to manage

the inaccuracies generated as radiations travel to the earth's surface and reflected. However, these issues have been worked on and currently, many satellite image providers now provide corrected images. For instance, it is now possible to download Top of Atmosphere (TOA) corrected Landsat TM, ETM+ and OLI images. Air temperature measurements usually taken at about 1.5 m above the ground using hand-held devices or equipment (sensors) mounted on vehicles and aircrafts (Kraaijenbrink et al., 2018; Wong & Yu, 2005) is also a viable alternative. However, the demerits of air temperature measurement approach seem to outweigh the limitations associated with satellite remote sensing based LST measurements.

Mirzaei & Haghighat, (2010) identified 3 significant limitations of air temperature measurements; a) the need for weather station data both within and outside the city which are oftentimes challenging to obtain; b) changes in instrumentation and data collection need to be considered in each microclimate; c) comparing central urban areas with the surrounding non-urban regions is a challenge, since many weather stations are usually situated close to airports which become urbanized over time. Hence, remote-sensing based measurements using satellite imagery seems to be the preferred approach to UHI studies.

The study of UHI based on LST deduced from satellite imagery requires an in-depth understanding of the nature of imagery available for use. Some currently available and widely used images containing Thermal-Infrared region (TIR) bands include NOAA, AVHRR, MODIS, ASTER, Landsat (MSS, TM, ETM+, OLI), SENTINEL-2A, and SENTINEL-3 SLSTR. These datasets come in different spatial and temporal resolutions broadly classified as high, medium or low resolutions. The fine (0.6 – 4 m), medium (4 – 30m) and low (30 m) resolution images do not have uniform band resolutions. In the bid to harmonise the trade-offs between image resolutions and data availability, it has been observed that most researches on UHI apply the medium resolution images containing TIR bands (Ngie et al., 2014). The Landsat, a widely used medium resolution multispectral image has its TIR on band 6 for MSS, TM and ETM+ although the spatial resolutions are 120m and 60m for the MSS and TM/ETM+ respectively. The TIR is captured in Bands 10 and 11 of the Landsat 8 (OLI) both at 100m resolutions. Similarly, SENTINEL-3 SLSTR's thermal-infrared ambient bands are S7, S8 and S9 bands (NASA, 2019). Other medium resolution data include ASTER with a 15m-resolution visible & near infrared (VNIR) data.

The broad approaches to the analyses of LST such as reference channel, emissivity normalisation, spectral ratios, alpha residuals methods are highlighted by Ngie et al., (2014). However, several improvements have been made in recent studies, especially for emissivity normalisation. For instance, the distribution pattern of LST has been studied in association with LULC surface types (Obiefuna et al., 2018; Surawar & Kotharkar, 2017). In these studies, the Normalized Difference Vegetation Index (NDVI), a measure of the extent of vegetation has been used to estimate spectral emissivity of data. This data together with the Top of Atmosphere Brightness Temperature (TOABT) can be used to calculate the LST using linear regression equations (Favretto, 2018). In this paper, preprocessed Top of Atmosphere (TOA) Landsat TM, ETM+ AND OLI images with <1 % cloud cover were sourced covering the 16 years from 2002 to 2018. The LULC changes

were detected using a pixel-based supervised classification approach. NDVI values were further estimated, and the LSTs for each map were derived. Subsequently, these results were used to establish the relationships between the LULC/degree of urbanisation and the UHI. The insights gained from the results are further discussed.

2. STUDY AREA

Nairobi county is located on latitude $1^0$16'59.99" S and longitude $36^0$49'0.01" E of the Greenwich meridian, slightly below the equatorial belt. It is one of the 47 counties in the country and the most-urbanised county. It is not just the nation's capital but, its city is the largest and most populous in Kenya. On the other hand, it is one of the smallest counties in terms of landmass covering only an area of 696 km^2 and is sub-divided into 17 sub-counties. Nairobi has over the years experienced rapid urban growth, and this growth is projected to continue at over 4% growth rate per annum which is well above the national average of approximately 3% per year (UNDESA, 2014). The county is home to over 6.5 million residents, and the current population density stands at about 4,850 residents per square km (World Population Review, 2019). It lies on the River Athi in the southern part of the country and has an average elevation of 1795m above sea level. Nairobi County can be described as a warm and temperate climate with a dry season in July – September and two rainy periods, April – May and November. The average rainfall is 869 mm, and the temperature is 19.0 ^{0}C. Figure 1 below shows a map of the study area.

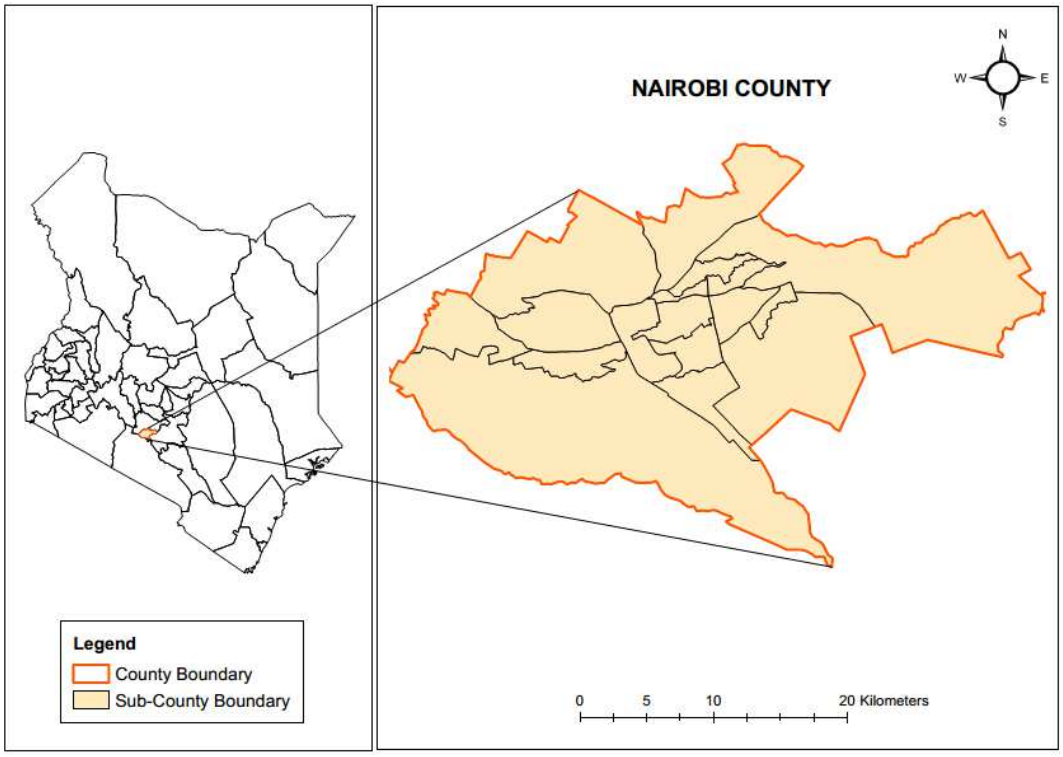

Figure 1: Map of Nairobi County

3. DATA AND METHODS

3.1. Data

In obtaining data for LULC classification and further analysis like the UHI studies, the importance of cloud-free images cannot be overemphasised. Hence cloud-free images (below 1%) with fairly even intervals were sourced. Details on the Landsat types and band characteristics are well documented in the literature (Barsi et al., 2014; USGS, 2018). Based on availability and fairly even interval of 2002, 2010 and 2018, the multitemporal images used in this study are; Landsat 5 TM (Thematic Mapper), Landsat 7 ETM + (Enhanced Thematic Mapper Plus) and Landsat 8 OLI (Operational Land Imager) images. The images were downloaded for path/row 168/061 from the USGS website and projected to WGS84 zone 37S UTM projection. Table 1 represents the summary of the information on the satellite imagery used in this study.

Table 1: Satellite Imagery Used in the Study

SN	Landsat Sensor	Acquisition date	Acquisition time	Sun Elevation	LULC Bands	Thermal Bands
1	Landsat 7 (ETM+)	10-02-2002	07:32:05	54.45805777	4(NIR), 3(Red), 2(Green)	6
2	Landsat 5 (TM)	19-08-2010	07:33:29	56.58427677	4(NIR), 3(Red), 2(Green)	6
3	Landsat 8 (OLI)	29-01-2018	07:43:05	55.92707521	5(NIR), 4(Red), 3(Green)	10 (TIRS 1), 11 (TIRS 2)

NIR – Near Infrared; TIRS – Thermal Infrared

The study area boundary shapefile was obtained from the Regional Centre of Mapping for Development (RCMD), Kenya in shapefile format.

3.2. Methods

The Landsat 7 (ETM+), Landsat 5 (TM) and Landsat 8 (OLI) obtained for the years 2002, 2010 and 2018 respectively were used to acquire land use/cover characteristics as well as land surface temperatures for each year. The boundary shapefile was used to clip the images into the area of interest before processing. Software used include; ENVI 5.3, Impact Tool and ArcGIS 10.3. ENVI 5.3 was used in land use/ land cover classification and the determination of land surface temperature. Impact tool which is an online based software was used to perform pre-processing on the raw images for LULC classifications. ArcGIS 10.3 was used in post classification editing and map layer production.

The study's methodology is summarised in Figure 2.

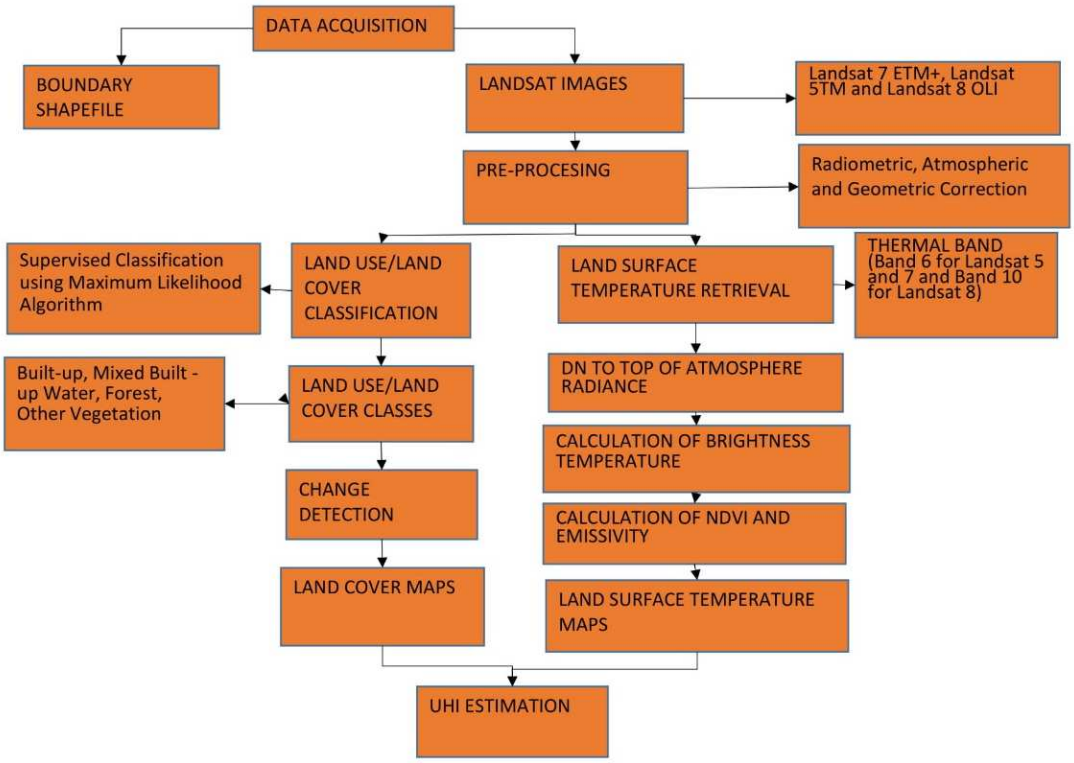

Figure 2: Study Methodology

3.2.1. Land Use/Land Cover Classification

Analysis of the land use/land cover (LULC) changes progressed with layer-stacking, followed by the pre-processing of the downloaded images using the impact tool for their radiometric and atmospheric corrections. A pixel-based supervised classification was done on the three images using Maximum likelihood algorithm in ENVI 5.3. Colour infrared band combination comprising the NIR, Red and Green bands were used for the LULC change detection and classification (Table 1). The identified five LULC categories based on the progression of urbanisation are; Built-Up, Mixed built-up, Other vegetation, Forest and water. Each category is briefly explained below;

Built-Up – Fully urbanised region, void of any green vegetation. Typical examples are downtown areas or central business districts of most major cities.

Mixed built-up – Urbanized area with few vegetative components like public spaces with some ornamental trees, shrubs and green playgrounds.

Other vegetation – This encompasses land cover classes like shrublands, grasslands, agricultural areas and general vegetative area that cannot be regarded as forests.

Forest – An area of land with over 10% tree canopy larger than 0.005 km^2 (0.5 ha), whose primary land use is not agricultural or other non-forest related land use.

Water – includes waterbodies such as rivers, perennial streams, lakes etc.

3.2.2. Land Surface Temperature

As highlighted in Table 1, Band 6 of the Landsat TM and ETM + and band 10 and 11 of Landsat 8 OLI were used for the assessment of the Land Surface Temperatures (LST). Band 10 was chosen based on the caution given by USGS on the potential unreliability of Band 11 in terms of calibration caused by stray light (USGS, 2019). The general methodology adopted in this study takes its cues from a wide range of studies (Avdan & Jovanovska, 2016; Favretto, 2018; Jiménez-Muñoz, 2003; Kaplan, Avdan, & Yigit Avdan, 2018; Lo & Quattrochi, 2003; Sobrino, Jiménez-Muñoz, & Paolini, 2004; Surawar & Kotharkar, 2017) and is represented by Figure 2.

The first step involved determining the Top of Atmosphere Spectral Radiance $L\lambda$. This was carried out using USGS formulas as shown in Avdan & Jovanovska, (2016). The second step involved the conversion of the $L\lambda$ to Brightness Temperature (BT). The conversion formula is as shown in (2) (Avdan & Jovanovska, 2016).

$$\mathrm{BT} = \frac{K_2}{\ln\left[(K_1/L\lambda) + 1\right]} - 273.15, \tag{1}$$

Where:
"BT = TOA Brightness Temperature, in Kelvin.
L_λ = Spectral radiance (Watts/ (m^{2*} sr * μm))
K1 =Thermal conversion constant for the band (from the metadata)
K2 =Thermal conversion constant for the band (from the metadata)"

The 273.15 in (1) indicates the conversion of the temperature values from degree kelvin into Celsius. The calibration constants K1 and K2 for Landsat 5TM and Landsat 7 ETM+ were obtained from the metadata and also shown in Chander & Markham, (2003).

The third step involved generating the Normalized Difference Vegetation Index (NDVI) for estimating the vegetation cover of the study area. The NDVI which ranges from -1.0 to +1.0 is essential for assessing the extent of vegetation cover of various land cover types. The formula for achieving this step is represented as Equation (2)

$$NDVI = \frac{NIR\ Band - R\ Band}{NIR\ Band + R\ Band} \tag{2}$$

Where; NIR is the near infrared band values for the multispectral image (Band 4 for TM and ETM+ and Band 5 for OLI); RED is the red band value of the image (Band 3 for TM and ETM+ and Band 4 for OLI). Calculation of NDVI is necessary to further calculate the proportion of vegetation (Pv) and emissivity (ε). Details of the role of NDVI in retrieving LST are well documented (Jiménez-Muñoz, 2003; Sobrino et al., 2004).

The fourth step involved the calculation of land surface emissivity using NDVI. The method adopted for emissivity calculation in this study was proposed by Zhang, Wang, & Li, (2006) and applied by Surawar & Kotharkar, (2017). It is worth noting that the land surface emissivity (LSE) is required to estimate LST. This is because LSE is a proportionality factor that calibates blackbody

radiance based on Planck's law to predict emitted radiance. It represents the efficiency of transmitting thermal energy into the atmosphere from the surface (Jiménez-Muñoz et al., 2009).

The fifth step was to calculate the LST using brightness temperature (BT) of bands 6 for Landsat TM and ETM+ and band 10 for Landsat 8 (OLI) and Land Surface Emissivity derived from NDVI. Land Surface Temperature was retrieved using (3).

$$T_s = \frac{\mathrm{BT}}{\{1 + [(\lambda \mathrm{BT}/\rho) \ln \varepsilon_\lambda]\}}, \tag{3}$$

Where, Ts is the Land Surface Temperature in Celsius (C℃), BT is at- sensor Brightness Temperature (℃), λ is the average wavelength of band 6 and 10 (for Landsat 5, 7 and 8 respectively), ελ is the emissivity. And ρ was calculated as shown in (4).

$$\rho = h\frac{c}{\sigma} = 1.438 \times 10^{-2}\ \mathrm{m\ K}, \tag{4}$$

Where σ is the Boltzmann constant (1.38×10^{-23} J/K), h is Planck's constant (6.626×10^{-34} Js), and c is the velocity of light (2.998×10^{8} m/s) (Weng, Lu, & Schubring, 2004). The LSTs were determined for each image, and the general trends in the datasets were observed. Different representative areas were selected for observation of point land surface temperatures for a more comprehensive comparison of the evolution of the LULC with the LST over the years observed. A comparison of the intensity of urban heat island from 2002 to 2018 was made to understand the changes in the temperature of Nairobi County.

3.2.3 Urban Heat Island

Identification of the UHI is based on the estimation of threshold temperatures as described in Ma, Kuang, & Huang, (2010) and applied by Kaplan et al., (2018): as follows

$LST > \mu + (0.5\ \sigma)$ - refers to UHI area

$0 < LST \leq \mu + (0.5\ \sigma)$ - denotes non-UHI areas

Where μ is the mean LST value of the study area, and σ is the standard deviation of the LST. The UHI intensity the further obtained by subtracting the LST of the referenced least urbanised area (forested) from that of the UHI area (Ma et al., 2010).

4. RESULTS AND DISCUSSION

The study throws some light on the progression of the LULC change of the study area over the 16-year period from 2002 to 2018 and how the LST has changed correspondingly over the same period. First, the general trend shows that progressive increases were observed in built-up and mixed built-up categories while other vegetation and forest categories experienced declines. Waterbody category, on the other hand, has only experienced slight changes tilting towards the positive. The summary of the LULC changes is represented in Table 2. It can be observed from Table 2 that built-up areas experienced the highest growth in the period under study with an overall increase of 7.29% between 2002 and 2018. Conversely, Forest cover experienced the highest

decrease in the same period with an overall decrease of 5.74%. A high progressive increase in built-up areas and a large matching decrease in forestland is perhaps the major contributor to the increase in UHI intensity in urban areas. Figure 3a-c represents the LULC maps.

Table 2 LULC Feature Classification

	LULC AREAS (km^2)						LULC Change Detection		
LULC Classes	**2002**	**2002 (%)**	**2010**	**2010 (%)**	**2018**	**2018 (%)**	**2002 – 2010 (%)**	**2010 – 2018 (%)**	**2002 – 2018 (%)**
Built-up	102.80	14.77	138.54	19.91	153.51	22.06	5.13	2.15	7.29
Mixed Built-up	93.32	13.41	102.67	14.75	116.69	16.77	1.34	2.01	3.36
Other Vegetation	320.66	46.07	305.47	43.89	286.12	41.11	-2.18	-2.78	-4.96
Forest	175.20	25.17	144.96	20.83	135.28	19.44	-4.34	-1.39	-5.74
Waterbody	4.02	0.58	4.35	0.62	4.41	0.63	0.05	0.01	0.06
TOTAL	**696**	**100.00**	**696**	**100.00**	**696**	**100.00**			

The daytime LST values are shown in Figure 4 a-c and represented in Tables 3. Twelve strategic observational points representative of the LULC features were taken across the study area. The computed threshold UHI temperatures and the corresponding daytime UHI intensities were also calculated as shown in Table 3.

Table 3 Variation of LST at representative points with changed LULC between 2002 and 2018

SN	Observation Location	LULC Feature	LST 2002	LST 2010	LST 2018
A	Mwiki	Built-up	31.76	26.15	35.24
B	Shauri Moyo Estate	Built-up	33.65	25.71	34.51
C	JKIA	Built-up	35.52	28.57	39.57
D	University of Nairobi	Mixed built-up	24.88	19.79	28.10
E	St. Mary's School Off Waiyaki Way	Mixed built-up	28.85	20.22	29.18
F	Kikuyu Road, Waithaka	Built-up	31.26	24.48	34.98
G	Nairobi City Park	Forest	24.87	17.60	26.66
H	Wastewater Plant, Eastern Bypass	Water	22.35	26.53	26.35
I	Karura Forest - ICRAF Road	Forest	23.86	16.26	24.85
J	Karura Environ	Other Vegetation	24.37	16.26	24.83
K	Karura Forest - From Kiambu Road	Forest	23.36	16.71	24.44
L	Nairobi National Park	Other Vegetation	30.09	23.22	35.59
		UHI Threshold	**30.15**	**24.22**	**33**
		Daytime UHI Intensity	**12.16**	**11.86**	**15.12**
Differences in UHI Intensity between 2002 and 2018					**2.96**

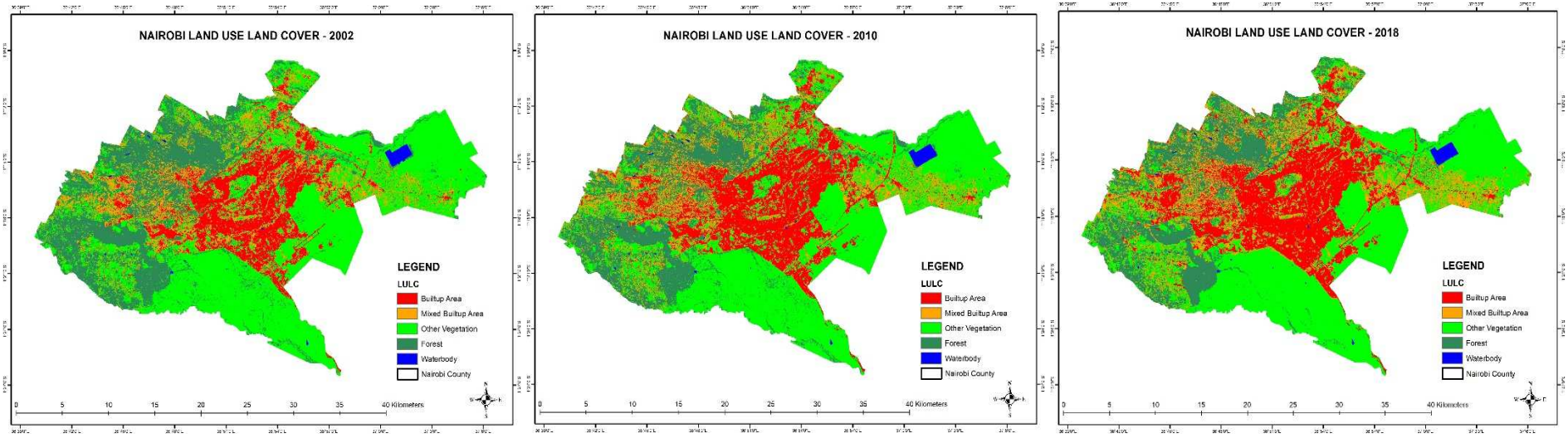

Figure 3: a) LULC 2002; b) LULC 2010; c) LULC 2018

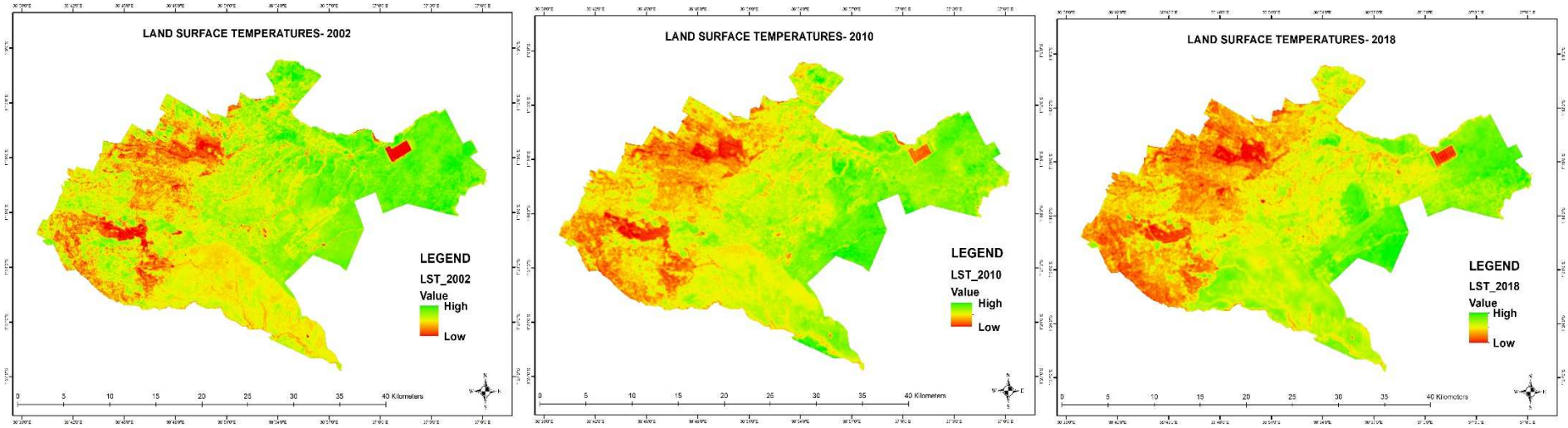

Figure 4: a) LST 2002; b) LST 2010; c) LST 2018

Firstly, it was observed that LST values taken in August 2010 were generally lower. This is likely because air surface temperatures in August are equally lower, as the coldest time of the year is the 3-month period from June to August (HWC, 2019). This finding implies that UHI is not static but more of a dynamic phenomenon which tends to increase during dryer and hotter months and tend to be lower in the colder months. It is worthy of note that Nairobi's daytime surface air temperatures (SAT) now peaks at values above 30 ℃ especially from January to March – the hottest times of the year (AccuWeather, 2019; HWC, 2019). Although Land Surface Temperatures are not the same as surface air temperatures, different studies have shown that there is a direct relationship between the two. The daytime LST has been observed to be generally higher than daytime SAT values especially in rougher terrains with a mean difference as high as 7 ℃ (Mutiibwa, Strachan, & Albright, 2015). This explains the relatively high values of the daytime LST with respect to the average surface air temperatures in the study area.

Table 3 shows built-up areas (points A, B, C, F) had consistently higher LST values than forested areas (points G, I, K). Also, the study shows that the LST of Nairobi increased at every observation point between 2002 and 2018 with Nairobi National Park experiencing the highest increase in LST from 30,09℃ to 35.50℃ (a 5.50℃ rise in temperature). The causes of the observed general increase in LST are likely to be a holistic one, encompassing not just increased urbanisation and generation of Greenhouse Gases but other broader concerns like climate change and deforestation. However, the role of urbanisation and anthropogenic influences are likely to have been substantial as depicted by the changes in LULC over the years. For instance, since urbanisation causes a decrease in pervious surfaces, engenders

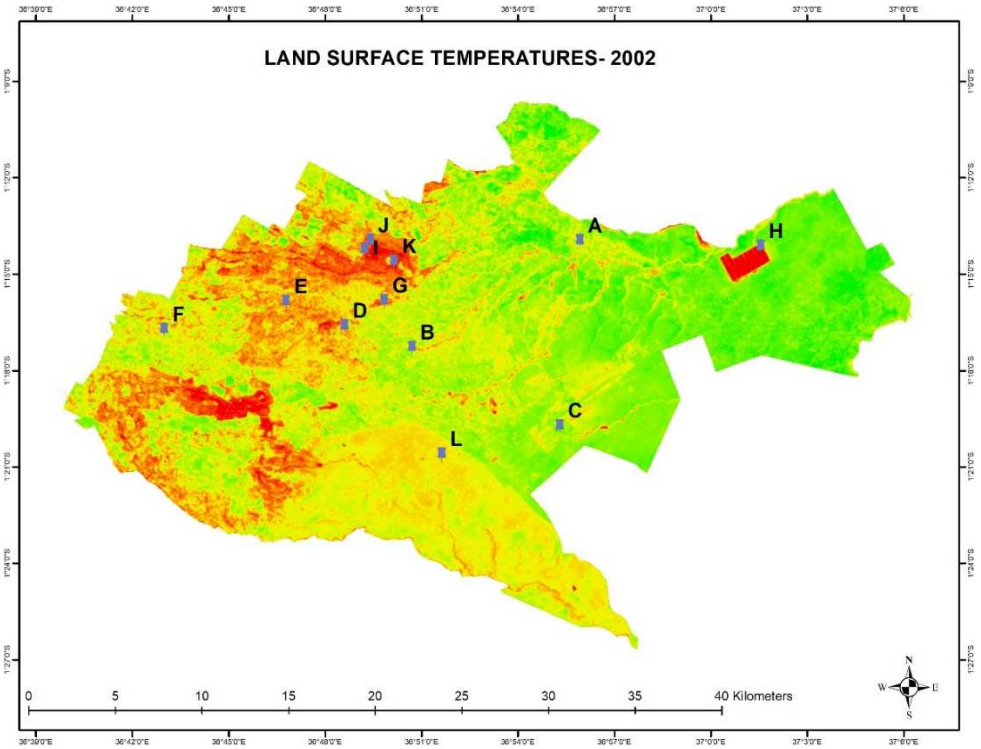

Fig 5: a) The LST map of the study area in 2002 showing the observation points

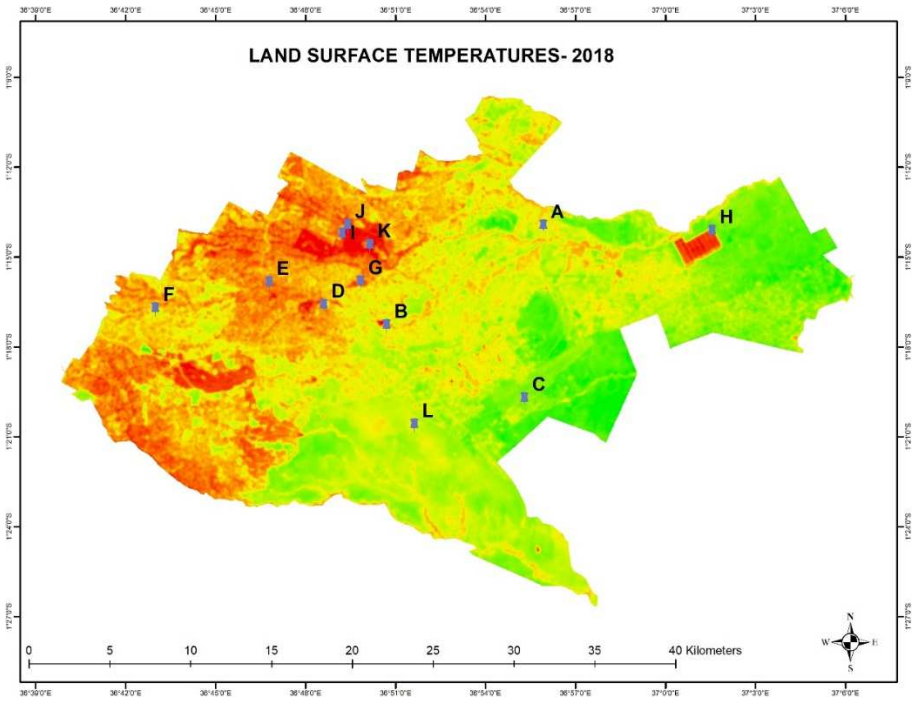

Fig 5: b) The LST map of the study area in 2018 showing the observation points

high industrial energy consumption, automobile exhaust emissions, domestic heating and decreases in vegetation and water surfaces, these ultimately alters the thermal conditions of the study area in various ways and thus affect the local temperature. The daytime UHI intensity was observed to increase by a value of 2.96 between 2002 and 2018 (Table 3). Some previous studies on UHI on the study area focused on portions of the city such as the Central Business District (Odongo, 2016); and Upper hill (Mwangi, Karanja, & Kamau, 2018). The studies considered short observation periods (2013/2014) and more extended periods from 1987 to 2017 (30 years) respectively. Another study by Oyugi, Karanja, & Odenyo, (2017) also observed the impact of LULC changes on surface temperatures from 1988 to 2015. An overarching conclusion from all these studies is that LST has been on the rise in Nairobi as also observed in the current study.

5. CONCLUSION AND RECOMMENDATION

This study shows that LULC in Nairobi County has changed from 2002 to 2018 with an increase of 7.29 % in built-up land, 3.36 % mixed built up and 0.06% in water bodies and decreases of 4.96% and 5.74% in forested and other vegetation areas respectively. Furthermore, urban growth trends implied an increase in LST from 2002 to 2018. Built-up areas represented by points A, B, C and F experienced a high rise in temperatures in comparison to forested areas represented by G, I, K. The highest increase in temperature was observed at Nairobi National Park with an LST increase from 30.00℃ to 35.50℃ (a 5.50℃ increase). This may be a cause for ecological concern for the national park as progressively high LST temperatures could put more stress on wildlife. The study also shows that UHI varies with months and tends to be highest in the peak of the dry season. The findings of this study, therefore, necessitates more concerted efforts towards achieving a greener environment. Lastly, further studies need to be done to provide a more detailed understanding of the impacts of urban morphology on UHI in the study area.

REFERENCES

AccuWeather. (2019). Nairobi, Kenya. Retrieved March 20, 2019, from https://www.accuweather.com/en/ke/nairobi/224758/daily-weather-forecast/224758

Akbari, H. (2005). *Energy Saving Potentials and Air Quality Benefits of Urban Heat Island Mitigation*. United States.

Aleksandrowicz, O., Vuckovic, M., Kiesel, K., & Mahdavi, A. (2017). Current trends in urban heat island mitigation research: Observations based on a comprehensive research repository. *Urban Climate*, *21*, 1–26.

Avdan, U., & Jovanovska, G. (2016). Algorithm for Automated Mapping of Land Surface Temperature Using LANDSAT 8 Satellite Data. *Journal of Sensors*. https://doi.org/10.1155/2016/1480307

Barsi, J. A., Lee, K., Kvaran, G., Markham, B. L., & Pedelty, J. A. (2014). The spectral response of the Landsat-8 operational land imager. *Remote Sensing*. https://doi.org/10.3390/rs61010232

Chander, G., & Markham, B. (2003). Revised Landsat-5 TM Radiometrie Calibration Procedures and Postcalibration Dynamic Ranges. *IEEE Transactions on Geoscience and Remote Sensing*. https://doi.org/10.1109/TGRS.2003.818464

EPA. (2019). Heat Island Impacts. Retrieved March 12, 2019, from https://www.epa.gov/heat-islands/heat-island-impacts

Favretto, A. (2018). Urban Heat Island analysis with Remote Sensing and GIS methods : an application in the Trieste area (North-East of Italy). *Bollettino Della Società Geografica Italiana Serie*, *1*(1), 215–229. https://doi.org/10.13128/bsgi.v1i1.101

Goldreich, Y. (2006). Ground and top of canopy layer urban heat island partitioning on an airborne image. *Remote Sensing of Environment*, *104.*, 247–255.

HWC. (2019). Nairobi, Kenya: Annual Weather Averages. Retrieved March 20, 2019, from https://www.holiday-weather.com/nairobi/averages/

Jiménez-Muñoz, J. C. (2003). A generalized single-channel method for retrieving land surface temperature from remote sensing data. *Journal of Geophysical Research*. https://doi.org/10.1029/2003jd003480

Jiménez-Muñoz, J. C., Sobrino, J. A., Plaza, A., Guanter, L., Moreno, J., & Martínez, P. (2009). Comparison between fractional vegetation cover retrievals from vegetation indices and spectral mixture analysis: Case study of PROBA/CHRIS data over an agricultural area. *Sensors*. https://doi.org/10.3390/s90200768

Kaplan, G., Avdan, U., & Yigit Avdan, Z. (2018). Urban Heat Island Analysis Using the Landsat 8 Satellite Data: A Case Study in Skopje, Macedonia. In *2nd International Electronic Conference on Remote Sensing, 22 March–5 April 2018* (p. 5171). MDPI. https://doi.org/10.3390/ecrs-2-05171

Kim, Y.-H., & Baik, J.-J. (2005). Spatial and temporal structure of the urban heat island in Seoul. *American Meteorological Society*, 591–605.

Kraaijenbrink, P. D. A., Shea, J. M., Litt, M., Steiner, J. F., Treichler, D., Koch, I., & Immerzeel, W. W. (2018). Mapping Surface Temperatures on a Debris-Covered Glacier With an Unmanned Aerial Vehicle. *Frontiers in Earth Science*, *6*(64), 1–19.

Lo, C. P., & Quattrochi, D. A. (2003). Urban Heat Island Phenomenon, and Health Implications : A Remote Sensing Approach. *PHOTOGRAMMETRIC ENGINEERING & REMOTE SENSING*, *69*(9), 1053–1063.

Ma, Y., Kuang, Y., & Huang, N. (2010). Coupling urbanization analyses for studying urban thermal environment and its interplay with biophysical parameters based on TM/ETM+ imagery. *International Journal of Applied Earth Observation and Geoinformation*. https://doi.org/10.1016/j.jag.2009.12.002

Madanian, M., Soffianian, A. R., Koupai, S. S., Pourmanafi, S., & Momeni, M. (2018). Analyzing the effects of urban expansion on land surface temperature patterns by landscape metrics: a case study of Isfahan city, Iran. *Environmental Monitoring and Assessment*, *190*(4).

Mirzaei, P. A., & Haghighat, F. (2010). Approaches to study Urban Heat Island – Abilities and limitations. *Buildings and Environment*, *45*, 2192–2201.

Mohajerani, A., Bakaric, J., & Jeffrey-Bailey, T. (2017). The urban heat island effect, its causes, and mitigation, with reference to the thermal properties of asphalt concrete. *Journal of Environmental Management*, *197:*, 522–538.

Mutiibwa, D., Strachan, S., & Albright, T. (2015). Land Surface Temperature and Surface Air Temperature in Complex Terrain. *IEEE Journal of Selected Topics in Applied Earth Observations and Remote Sensing*, *8*(10), 4762–4774. https://doi.org/10.1109/JSTARS.2015.2468594

Mwangi, P. W., Karanja, F. N., & Kamau, P. K. (2018). Analysis of the Relationship between Land Surface Temperature and Vegetation and Built-Up Indices in Upper-Hill, Nairobi. *Journal of Geoscience and Environment Protection*, *6*, 1–16. https://doi.org/10.4236/gep.2018.61001

NASA. (2019). Copernicus Sentinel-3 Sea and Land Surface Temperature Radiometer (SLSTR). Retrieved March 11, 2019, from https://ladsweb.modaps.eosdis.nasa.gov/missions-and-measurements/slstr/

Ngie, A., Abutaleb, K., Ahmed, F., Darwish, A., & Ahmed, M. (2014). Assessment of urban heat island using satellite remotely sensed imagery : a review. *South African Geographical Journal*. https://doi.org/10.1080/03736245.2014.924864

Obiefuna, J. N., Nwilo, P. C., Okolie, C. J., Emmanuel, E. I., & Daramola, O. (2018). Dynamics of Land Surface Temperature in Response to Land Cover Changes in Lagos Metropolis. *Nigerian Journal of Environmental Sciences and Technology*, *2*(2), 148–159.

Odongo, S. O. (2016). *URBAN HEAT ISLAND: INVESTIGATION OF URBAN HEAT ISLAND EFFECT. A Case Study of Nairobi.* University of Nairobi.

Oke, T. R. (1973). City size and the urban heat island. *Atmospheric Environment*, *7*(8), 769–779.

Oyugi, M. O., Karanja, F. N., & Odenyo, V. A. O. (2017). Modelling the Effect of Land Use and Land Cover Variations on the Surface Temperature Values of Nairobi City, Kenya. *Resources and Environment*, *7*(6), 145–159. https://doi.org/10.5923/j.re.20170706.01

Rinkesh. (2019). What is Urban Heat Island? Retrieved from https://www.conserve-energy-future.com/effects-solutions-urban-heat-island.php

Sobrino, J. A., Jiménez-Muñoz, J. C., & Paolini, L. (2004). Land surface temperature retrieval from LANDSAT TM 5. *Remote Sensing of Environment*. https://doi.org/10.1016/j.rse.2004.02.003

Surawar, M., & Kotharkar, R. (2017). Assessment of Urban Heat Island through Remote Sensing in Nagpur Urban Area Using Landsat 7 ETM + Satellite Images. *International Journal of Urban and Civil Engineering*, *11*(7), 868–874.

UN. (2018). 68% of the world population projected to live in urban areas by 2050, says UN. Retrieved February 2, 2019, from https://www.un.org/development/desa/en/news/population/2018-revision-of-world-urbanization-prospects.html

UNDESA. (2014). *World Urbanization Prospects*. *Undesa*. https://doi.org/10.4054/DemRes.2005.12.9

USGS. (2018). What are the band designations for the Landsat satellites? Retrieved December 5, 2018, from https://landsat.usgs.gov/what-are-band-designations-landsat-satellites

USGS. (2019). How are the Thermal Infrared Sensor (TIRS) thermal bands aboard Landsat 8 used? Retrieved from https://landsat.usgs.gov/how-are-thermal-infrared-sensor-tirs-thermal-bands-aboard-landsat-8-used

Voogt, J. A., & Oke, T. R. (2004). Thermal Remote Sensing of Uran areas. *Remote Sensing of Environment*, 370–384.

Weng, Q., Lu, D., & Schubring, J. (2004). Estimation of land surface temperature-vegetation abundance relationship for urban heat island studies. *Remote Sensing of Environment*. https://doi.org/10.1016/j.rse.2003.11.005

Wong, N. H., & Yu, C. (2005). Study of green areas and urban heat island in a tropical city. *Habitat International*, *29*, 547–558. https://doi.org/10.1016/j.habitatint.2004.04.008

World Population Review. (2019). Nairobi Population 2019. Retrieved March 13, 2019, from http://worldpopulationreview.com/world-cities/nairobi-population/

Zhang, J., Wang, Y., & Li, Y. (2006). A C++ program for retrieving land surface temperature from the data of Landsat TM/ETM+ band6. *Computers and Geosciences*. https://doi.org/10.1016/j.cageo.2006.05.001

Zhang, Z., Ji, M., Shu, J., Deng, Z., & Wu, Y. (2008). SURFACE URBAN HEAT ISLAND IN SHANGHAI, CHINA : EXAMINING THE RELATIONSHIP BETWEEN LAND SURFACE TEMPERATURE AND IMPERVIOUS SURFACE FRACTIONS DERIVED FROM LANDSAT ETM + IMAGERY. *The International Archives of the Photogrammetry, Remote Sensing and Spatial Information Sciences*, *37*(B8), 601–606.